Analysis of *b*-value and improved *b*-value of acoustic emissions accompanying rock fracture

M. V. M. S. Rao* and K. J. Prasanna Lakshmi

National Geophysical Research Institute, Hyderabad 500 007, India

Acoustic emissions (AE) produced during the compressive fracture of a brittle rock have been subjected to detailed analysis using an advanced software for the computation of *b*-value as well as improved *b*-value. Conventionally, the *b*-value of AE is calculated using the Gutenberg–Richter relationship, which is widely used in seismology. Determination of improved *b*-value is a new approach, which is computed from AE amplitude distribution data. It involves filtering of high and low amplitude AE hits (or events) in a selective manner. The results obtained by both these methods to evaluate the fracture process in the rock are compared and discussed.

Keywords Acoustic emission, *b*-value, GBR relationship, improved *b*-value, rock fracture.

STRESS waves produced by dynamic processes in materials are known as acoustic emissions (AE). AE occur as a release of a series of short, impulsive energy packets and travel as spherical wavefronts in the material under stress. There can be many sources of AE, but the most important one is from micro-cracking as far as brittle materials are concerned[1–5]. One of the most interesting observations is that a close analogy exists between AE produced from materials undergoing brittle failure at the laboratory scale and seismic waves caused due to earthquakes[6]. This fact has motivated non-destructive testing (NDT) specialists to develop and refine the AE technique such that it can serve as an NDT tool for monitoring and understanding the mechanisms of dynamic processes and also to forewarn the impending failure in engineering materials including rocks at several scales and earthquakes[7,8].

Among various parameters, the most significant one is the *b*-value which is derived from the amplitude distribution data of AE following the methods used in seismology[9–11]. The *b*-value is defined as the 'log-linear slope of the frequency–magnitude distribution' of AE[12–18]. It represents the 'scaling of magnitude distribution' of AE, and is a measure of the relative numbers of small and large AE which are signatures of localized failures in materials under stress. While testing the materials undergoing brittle failure, the *b*-value is found to range from 1.5 to 2.5 in the initial stages. It then decreases with increase in stress to attain values ≈ 1.00 and less, showing temporal fluctuations as the impending failure approaches in the material[16–21]. A high *b*-value arises due to a large number of small AE hits (or events) representing new crack formation and slow crack growth, whereas a low *b*-value indicates faster or unstable crack growth accompanied by relatively high amplitude AE in large numbers. In earthquake seismology also, values of unity (1.00) are common for seismic *b*-value, and a systematic study of temporal changes in it has shown that large earthquakes are often preceded by an intermediate increase in *b*-value, followed by a decrease in the months to weeks before the earthquake[8–11]. Thus there are good prospects for making a quantitative diagnosis of the fracture development in the test solid or structure under stress on the basis of AE amplitude information in terms of *b*-value. However, the method used for the determination of *b*-value is important, since selection of the amplitude or magnitude limits of the 'linear range' of the cumulative frequency distribution data of AE is critical. Some improvizations have been attempted in recent years to fine-tune the amplitude distribution graph and use the mean amplitude and standard deviation of the amplitude distribution for computing the improved *b*-value (or I*b*-value) and use it for the evaluation of slope failure and fracture process in concrete, etc.[22–24]. Here results of *b*-value and I*b*-value of AE generated during the deformation and failure of a granite rock sample under uniaxial compression are compared and discussed.

Experimental

We carried out uniaxial compression tests and monitored the deformation and failure behaviour of a set of Godhra granites from Panchamahals district, Gujarat[25]. The tests were carried out by incrementing the stress at a constant rate on the test sample using a servo-controlled testing machine, and by recording the strain and AE concurrently. The multiparameter AE data, including hits, ring-down counts and amplitudes were obtained using a PC-based AE system (Spartan of PAC, USA). The time duration of the test was 1080 s and the uniaxial compressive strength[25] of the test

*For correspondence. (e-mail: mvmsrao@ngri.res.in)

sample was 229.27 MPa. The recorded data of the amplitude distributions of AE hits corresponding to successive non-overlapping stress/time windows have been processed and the cumulative frequency–amplitude distribution graphs have been obtained using Mistras software (PAC, USA). Figure 1 shows cumulative number of AE hits on the vertical log scale and amplitude of AE in dB on the horizontal scale. The threshold (A_T) was set at 45 dB in our experiments and all the AE were found to fall in the amplitude range of 45 to 100 dB. A large number of AE hits had smaller amplitudes and the distribution shows a descending gradient (Figure 1). The slope of the 'linear descending branch' of the cumulative distribution graph is the *b*-value of AE after applying the necessary correction for the following reasons. Data of *b*-value and I*b*-value of all the individual subsets of AE have been obtained by applying the Gutenberg–Richter[9] relationship and its modified version.

Computation of b-value and results

The *b*-value is usually computed using the 'cumulative frequency–magnitude' distribution data and applying the Gutenberg–Richter relationship[9], which is widely used in seismology. The equation is as follows:

$$\log_{10} N = a - bM, \tag{1}$$

where M is the Richter magnitude of earthquakes, N the incremental frequency (i.e. the number of earthquakes with magnitude greater than M), a an empirical constant and b is the *b*-value which is mostly ~1.0. The standard error in b is $b/\sqrt{n}$ for a sample number of n earthquakes and 95% confidence limits are twice this value[11]. M is proportional to the logarithm of the maximum amplitude (A_{max}) recorded in a seismic trace and also to the logarithm of the source rupture area (S)[9–11]. Equation (1) has been found to be valid for the AE data also to compute the AE *b*-value after dividing the AE amplitude by a factor of 20, because of the fact that the AE peak amplitude is measured in dB, whereas the Richter magnitude of earthquake is defined in terms of the logarithm of maximum amplitude[16–18]. In terms of AE technique, the Gutenberg–Richter formula therefore gets modified as:

$$\log N = a - b(A_{dB}/20), \tag{2}$$

where N is the incremental frequency (i.e. the number of AE hits with amplitude greater than the threshold A_T), a an empirical constant and b the *b*-value[17,21]. An important issue is the selection of the 'linear descending branch' of the cumulative frequency–amplitude distribution graph, because it shows deviations from linearity in the low and high amplitude ranges, as shown schematically in Figure 2. Therefore, the lower and upper amplitude limits of the linear range, namely a_1 and a_2 have to be selected either from the graph to compute the *b*-value or using a special software that calculates the mean amplitude and RMS deviation of each AE subset and yields the *b*-value[22–24].

The results of the present study show that the cumulative frequency–amplitude distribution graphs show a fairly good linear relationship (Figure 1). However, there is a marked change in the trend of the amplitude distribution after the onset of dilatancy (inelastic volume change due to microcracking) in the rock at ~66.5% failure stress, as discussed in detail by Rao *et al.*[25]. The mean amplitude of AE of the individual subsets was found to increase gradually with

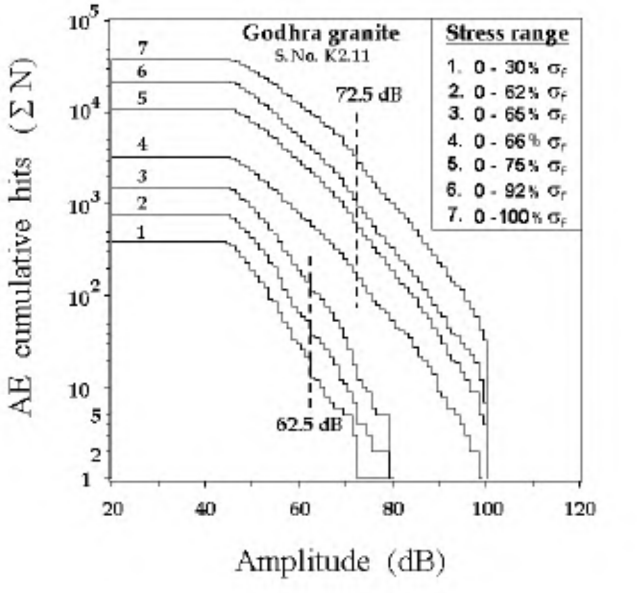

Figure 1. AE cumulative frequency–amplitude distribution graphs corresponding to different stress ranges. The graphs were obtained from the replay of AE amplitude data recorded during deformation and progressive failure of a granite rock sample (K2.11) under uniaxial compression. UCS (σ_f) of the tested rock was 229.27 MPa. Mean amplitude and trend of the distribution graph changed significantly from 62.5 to 72.5 dB with the onset of dilatancy at ~66% failure stress.

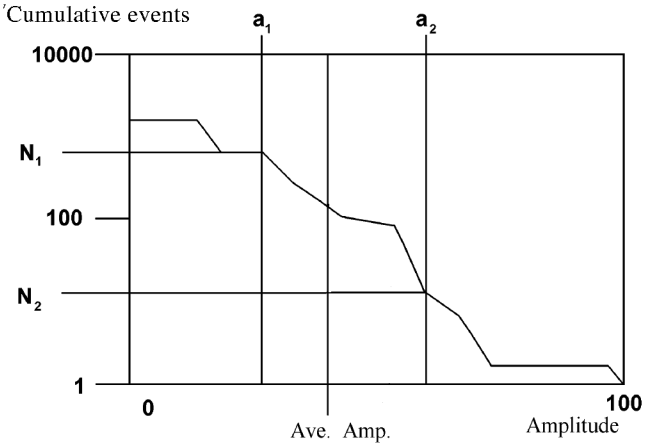

Figure 2. Schematic diagram showing descending gradient of cumulative frequency distribution of AE amplitude (Source: Ref. 24).

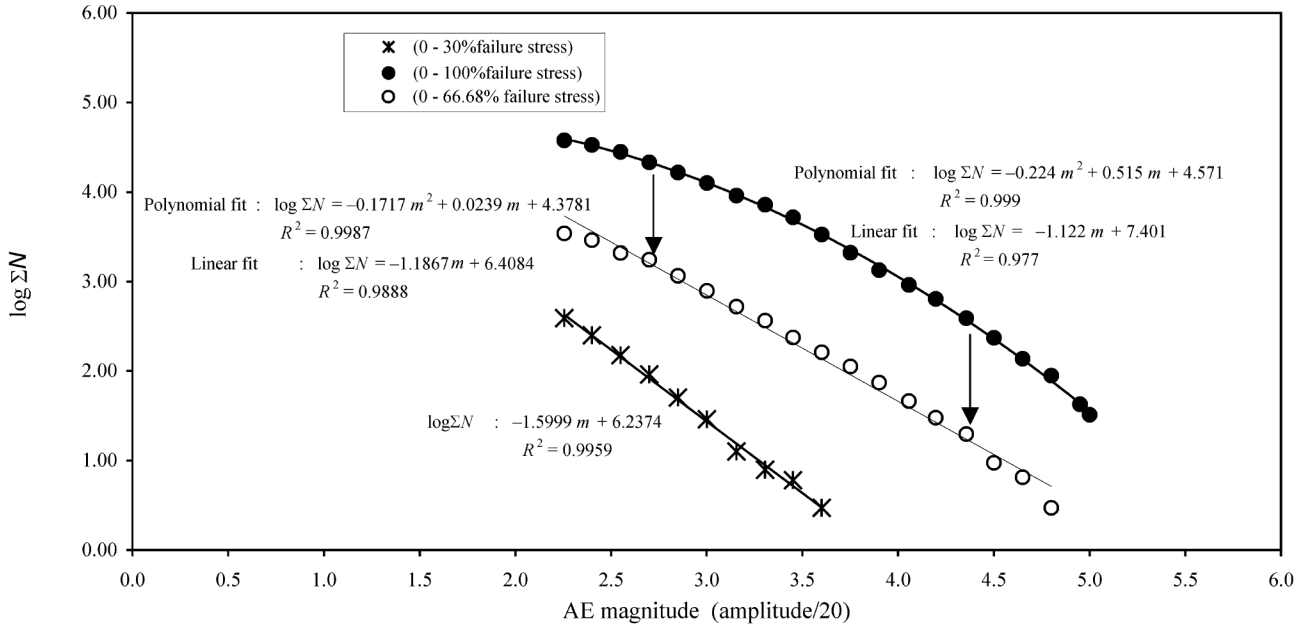

Figure 3. Cumulative frequency–magnitude distribution plots of AE corresponding to three stress ranges. Data were generated during progressive failure of a Godhra granite rock (S. no. K2.11) under uniaxial compression. Distribution is linear during early stages of loading and appears more as a polynomial curve at stresses near failure. However, the distribution graph shows a 'fairly good linear relationship' in the magnitude range from 2.7 to 4.4, as indicated by arrows.

increase in stress. It was found to be ~ 62.5 dB during the initial stages up to dilatancy and reached ~ 72.5 dB with the onset of dilatancy at 66.5% failure stress (Figure 1). Another interesting feature is that the AE amplitude distributions do not show a single straight line, and different ranges of amplitude might give different lines. This can be seen clearly in Figure 3, where a few sets of 'cumulative AE-magnitude distribution' graphs are shown after applying the necessary correction to convert AE amplitude to magnitude. In the initial stages when the stress range is low (0–30% failure stress) and when the AE population is less, the cumulative AE hit-magnitude distribution plot is fully linear (Figure 3). Whereas in the higher stress ranges (stresses > 66.5% failure stress), the cumulative AE hit-magnitude distribution graph shows a 'fairly good linear relationship' in the magnitude range from 2.70 to 4.40, although the polynomial fit yields better correlation (Figure 3). The corresponding lower and upper limiting ranges of AE amplitude are 54 and 88 dB. The *b*-value of individual subsets has been obtained taking the AE hit data with the number of samples ~ 250–500 at lower stress levels and ~ 50 at higher stress levels corresponding to that range (magnitude: 2.7 to 4.4) and using linear regression analysis and eq. (2). The results are shown plotted as *b*-values (GBR) against the failure stress in Figure 4 *a* (0–100% failure stress) and Figure 4 *b* (60 to 100% failure stress) along with I*b*-values (PAC) which are discussed later. The results show sharp changes in *b*-value corresponding to the various stages of rock deformation and formation and growth of stable cracks, unstable cracks and crack coalescence, which are marked in the plots and also listed in Figures 4 *a*, *b*. The details are discussed later and compared with the inferences drawn from the results of stress-induced changes in I*b*-value.

Computation of Ib-value and results

Since amplitude distributions of AE vary during the test, statistical values such as mean and standard deviation of each amplitude set are taken into account and an 'improved *b*-value' (I*b*) was proposed and applied to evaluate slope failure[22] and also the fracture process in concrete[23]. The I*b*-value was defined as:

$$Ib = [\log N(\mu - \alpha_1\sigma) - \log N(\mu + \alpha_2\sigma)]/[(\alpha_1 + \alpha_2)]\sigma, \quad (3)$$

where μ is the mean amplitude, σ the standard deviation, and α_1 and α_2 are user-defined constants which would represent coefficients of lower and upper limits of the amplitude range to yield a proper straight line. When a comparison between seismic *b*-value and I*b*-value is to be made, the I*b*-value should be multiplied[23] by 20. Following this, the Physical Acoustics Corporation (PAC) had come out with a software[24] to compute the I*b*-values after the peak amplitude limits (a_1 and a_2) of the linear descending distribution of AE hits have been selected (Figure 1), using the mean amplitude and standard deviation of each subset of AE. The formula proposed by PAC is as follows:

$$Ib = (\log N_1 - \log N_2)/(a_2 - a_1), \quad (4)$$

where N_1 and N_2 correspond to cumulative AE hits at the lower amplitude limit (a_1) and upper amplitude limit (a_2) respectively, of each amplitude distribution graph (such as Figure 1) respectively. The new program package facilitates computation and plotting of I*b* using either amplitude distribution data or energy distribution data of selected number of AE hits (or events). The user has the option to set the number of data samples and values of a_1 and a_2 either directly in the program or using the mean amplitude (μ), standard deviation (σ) and setting different values ranging from 0.5 to 5.0 for α_1 and α_2 as follows, to obtain the values of I*b* using eq. (4).

$$a_1 = \mu - \alpha_1\sigma \quad \text{and} \quad a_2 = \mu + \alpha_2\sigma. \quad (5)$$

For the present study, we have obtained μ and σ of each AE amplitude distribution graph using standard methods of statistics and computed I*b* using eqs (3)–(5). σ was found to be ~ 9 dB for most of the AE amplitude datasets. However, the mean amplitude of AE (μ) increased linearly from 51 to 60 dB with increase in stress up to 42% failure stress (i.e. stages I and II). It was then found to in-

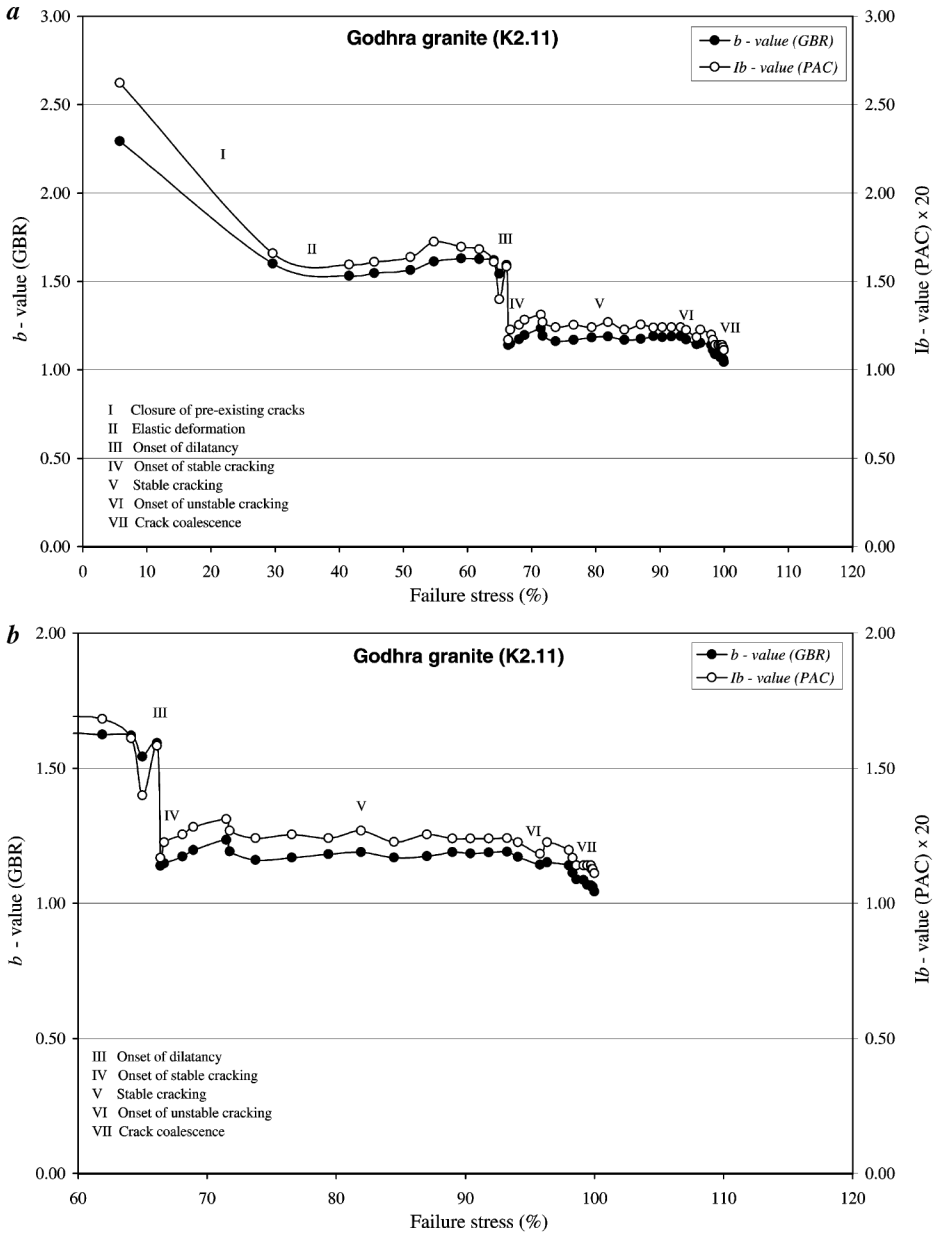

Figure 4. ***a***, The *b*-value (GBR) and I*b*-value (PAC) plotted against uniaxial compressive stress (0–100% failure stress). Various stages at which sharp changes in *b*-value and I*b*-value have occurred and inferences drawn from them are also shown. ***b***, same as in (***a***), but stress range is set from 60–100%.

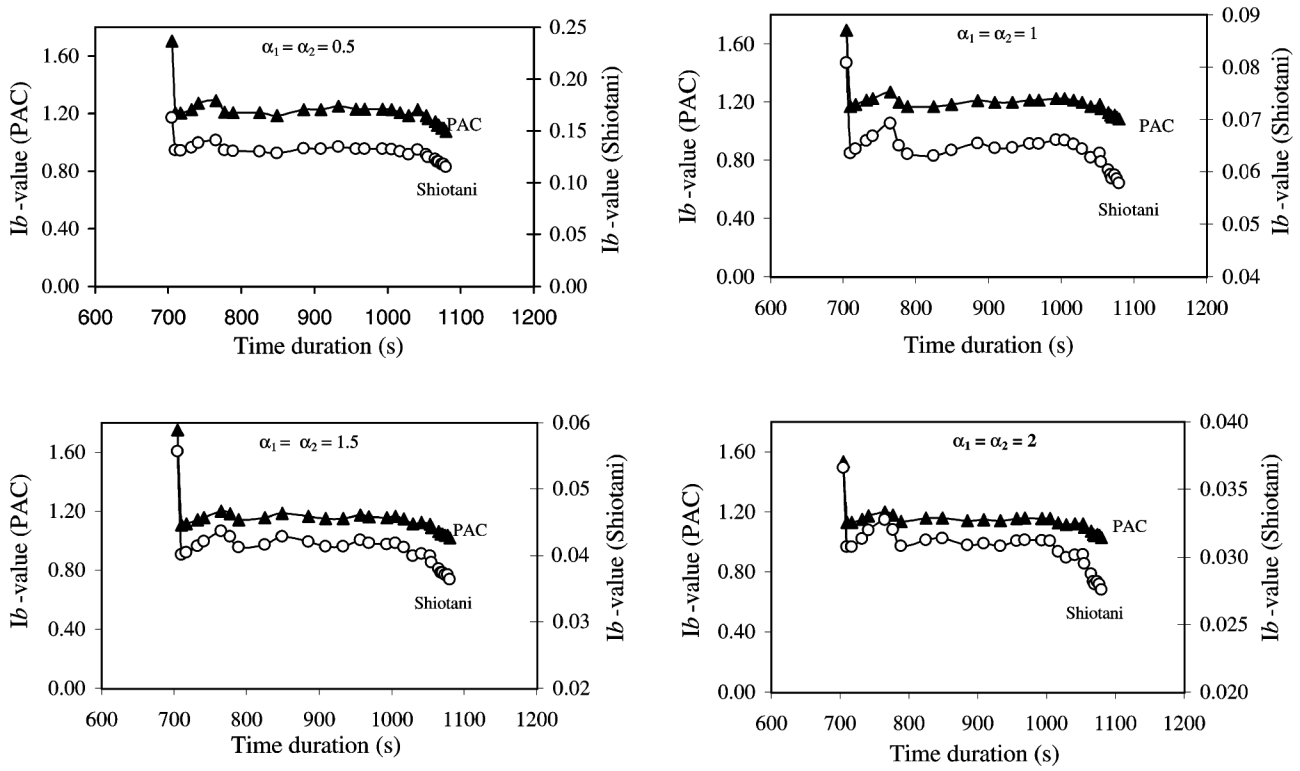

Figure 5. Plot showing comparison of trends of temporal variations in I*b*-value of AE of Godhra granite (S. no. K2.11). I*b*-values (PAC) computed from eqs (4) and (5), and I*b*-values (Shiotani) computed from eq. (3) are multiplied by 20 and plotted against time duration. (For details see the text.)

crease sharply to 69 dB due to the formation of a large number of new micro-cracks and the onset of dilatancy (stage III). With further increase in stress, the mean amplitude increased to 72 dB at 72% failure stress and remained constant until the final failure occurred in the sample. We have used values ranging from 0.5 to 2 for α_1 and α_2, and considered that $\alpha_1 = \alpha_2$ for computing I*b*-values of AE for different stages. The values thus obtained from eqs (3) and (4) have been designated as I*b* (Shiotani) and I*b* (PAC) respectively, for this study. The I*b* (Shiotani) values and the I*b* (PAC) values were multiplied by 20, as suggested by Shiotani *et al.*[23] in order to compare them with the *b*-values obtained using eq. (2). The results are shown in Figure 5 in which the corrected values of I*b* (PAC) and I*b* (Shiotani) for different sets of α are plotted as a function of the time duration of the test. The results show that I*b* (Shiotani) is lower by an order of magnitude than I*b* (PAC) for all values of α, although it shows a similar trend as that of PAC (I*b*) with regard to its temporal changes (Figure 5). Furthermore, values of I*b* (PAC) are ~ 1.00 for all values of α (Figure 5). The results show that when $\alpha_1 = \alpha_2 = 1$, agreement between *b* and I*b* (PAC) is particularly more close, as can be seen in Figure 4 *a* and *b*. The lower and upper amplitude limits in that case become 63 and 81 dB with a mean amplitude of 72 dB and standard deviation ~ 9.0 dB. On the other hand, I*b* (Shiotani) is found to be far below the *b*-value (GBR) and I*b* (PAC).

Discussion

The results show that during the early stages of loading (stages I and II), AE generated due to the closure and rubbing of pre-existing micro-cracks in the rock began to show a high *b*-value (GBR) of ≈ 2.25 and high I*b*-value (PAC) of ≈ 2.62. It then decreased to ≈ 1.53 and ≈ 1.59 respectively, and stabilized during the elastic deformation stage (stage II) of the rock (Figure 4 *a*). At the end of that stage, dilatancy (inelastic volume change) begins due to the formation of a large number of new micro-cracks on the eventual fracture plane. In the present study it was found to be quite sudden and it took place at ~ 66.5% failure stress with both *b*-value (GBR) and I*b* (PAC) value decreasing sharply and also appreciably to 1.15 and 1.17 respectively (Figure 4 *a*, *b*, stage III). With further increase is stress, the *b*-value (GBR) and I*b*-value (PAC) increased slightly, marking the transition from 'formation' to 'growth' stage of the newly formed cracks (Figure 4 *b*, stage IV). The newly formed cracks began to grow stably in number and size on the eventual fracture plane of the test rock, i.e. stage V during which the *b*-value (GBR) and I*b*-value (PAC) remained more or less constant until ≈ 94% failure stress. Then it was followed by the onset of unstable cracking (stage VI) as a result of which the *b*-value (GBR) and I*b*-value (PAC) decreased until the applied stress reached a value of ≈ 98% failure stress (Figure 4 *b*). The coalescence

of cracks commenced at stage VII due to closer crack spacing. Then the *b*-value (GBR) and I*b*-value (PAC) began to decrease sharply due to crack coalescence and the accompanying stress relief, and at the final failure they had fallen to as low as 1.04 and 1.11 respectively. For all practical purposes, the transitions from stage V to stage VI and from stage VI to stage VII can be considered as most useful for the identification of critical state of damage and prediction of failure time of the test rock. At and around those critical stages, if the *b*-value and I*b*-value can be determined for fixed number of hits with moving average window method, the results will be more advantageous.

Concluding remarks

Though the computation and application of I*b*-value is a new approach using the 'mean and standard deviation' of the amplitude distribution data of AE, the results of the present study show that a suitable correction factor (multiplication by 20) is required to be applied to make the I*b*-value (PAC) comparable to the universally accepted *b*-value of 1.00. On the other hand, determination of *b*-value using the GBR relationship adoptable to AE directly and applying the regression analysis for the 'linear descending gradient' is more straightforward and useful for investigating the fracture development in brittle materials such as rocks. In the present study, the AE sampled and characterized in terms of *b*-value at stresses close to failure clearly indicated the onset of 'unstable cracking' as well as 'crack coalescence' leading to dynamic failure of the rock. These observations have some vital applications for monitoring the stability and integrity of rocks at several scales.

1. Liptai, R. G. and Harris, D. O., Acoustic emission – An introductory review. *Mater. Res. Stand.*, 1971, **11**, 1–4.
2. Ono, K. (ed.), In *Fundamentals of Acoustic Emission*, UCLA Publ., Los Angeles, USA, 1979.
3. Baldev Raj and Jha, B. B., Acoustic emission – I. Fundamentals of acoustic emission. *J. Non-Destr. Eval.*, 1992, **12**, 37–47.
4. Murthy, C. R. L., Bhat, M. R. and Ravishankar, S. R., Evaluation of composite materials and structures by acoustic emission. *J. Non. Destr. Eval.,* 1995, **15**, 100–105.
5. Rao, M. V. M. S., Acoustic emission signatures of rocks and concrete stressed to failure in compression under laboratory conditions. In Proc. 4th National Workshop on Acoustic Emission (NAWACE-97), Mumbai, August 1997, pp. 31–41.
6. Lockner, D., The role of acoustic emission in the study of rock fracture. *Int. J. Rock Mech. Min. Sci. Geomech. Abstr.*, 1993, **30**, 883–899.
7. Hardy Jr., H. R., Application of acoustic emission techniques to rock mechanics research. ASTM STP 505, ASTM Publ., Philadelphia, USA, 1972.
8. Lockner, D., Brittle fracture as an analog to earthquakes: Can acoustic emission be used to develop a viable prediction strategy. *J. Acoust. Emission*, 1996, **14**, S88–S101.
9. Gutenberg, B. and Richter, C. F., In *Seismicity of the Earth and Associated Phenomena*, Princeton University Press, Princeton, NJ, USA, 1954, 2nd edn.
10. Aki, K., Maximum likelihood estimates of *b* in the formula log*N* = *a* – *bm* and its confidence limits. *Bull. Earthquake Res. Inst., Tokyo Univ.*, 1965, **43**, 237–239.
11. Smith, W. D., The *b*-value as an earthquake precursor. *Nature*, 1981, **289**, 136–139.
12. Mogi, K., Magnitude–frequency relation for elastic shocks accompanying fracture of various materials and some related problems in earthquakes. *Bull. Earthquake Res. Inst., Tokyo Univ.*, 1962, **40**, 831–853.
13. Nakamura, Y., Veach, C. L. and McCauley, B. O., Amplitude distribution of acoustic emission signals. In ASTM Special Technical Publication, Philadelphia, 1962, vol. 505, pp. 164–186.
14. Scholz, C. H., The frequency–magnitude relation of microfracturing and its relation to earthquakes. *Bull. Seismol. Soc. Am.*, 1968, **58**, 399–417.
15. Pollock, A. A., Acoustic emission amplitudes. *Non.-Destr. Test. (Guildford, Engl.)*, 1973, 264–269.
16. Cox, S. J. D. and Meredith, P. G., Microcrack formation and material softening in rock measured by monitoring acoustic emission. *Int. J. Rock Mech. Min. Sci. Geomech. Abstr.*, 1993, **30**, 11–21.
17. Hatton, C. G., Main, I. G. and Meredith P. G., A comparison of seismic and structural measurements of scaling exponents during tensile sub-critical crack growth. *J. Struct. Geol.*, 1993, **15**, 1485–1495.
18. Rao, M. V. M. S., Significance of AE-based *b*-value in the study of progressive failure of brittle rock: Some examples from recent experiments. In Proc. 14th World Conference on Non-Destructive Testing (14th WCNDT), (eds Krishnadas Nair, C. G. *et al.*), Oxford & IBH, New Delhi, Dec. 1996, vol. 4, pp. 2463–2467.
19. Sammonds, P. R., Meredith, P. G. and Main, I. G., Role of pore-fluids in the generation of seismic precursors to shear fracture. *Nature*, 1992, **359**, 228–230.
20. Lei, X., Kusunose, K., Rao, M. V. M. S., Nishizawa, O. and Satoh, T., Quasi-static fault growth and cracking in homogeneous brittle rocks under triaxial compression using acoustic emission monitoring. *J. Geophys. Res.*, 2000, **105**, **B3**, 6127–6139.
21. Colombo, I. S., Main, I. G. and Ford, M. C., Assessing damage of reinforced concrete beam using *b*-value analysis of acoustic emission signal. *J. Mat. Civ. Eng.*, 2003, **15**, 280–286.
22. Shiotani, T., Fujii, K., Aoki, T. and Amou, K., Evaluation of progressive failure using AE sources and improved *b*-value on slope model tests. *Prog. Acoust. Emission*, 1994, **VII**, 529–534.
23. Shiotani, T., Yuyama S., Li, Z. W. and Ohtsu, M., Application of the AE improved *b*-value to qualitative evaluation of fracture process in concrete materials, *J. Acoust. Emission*, 2001, **19**, 118–132.
24. Physical Acoustics Corporation (PAC), *b*-value Software Option – User's Manual, May 2002, pp. 1–6.
25. Rao, M. V. M. S., Murthy, D. S. N., Nagaraja Rao, G. M., Mohanty, S. K. and Udaya Kumar, S., Stress-induced micro-cracking and brittle failure of Godhra granite. *J. Geol. Soc. India*, 2004, **64**, 775–783.

ACKNOWLEDGEMENTS. Financial assistance received from the Department of Science and Technology, New Delhi is acknowledged. We thank Dr V. P. Dimri, Director, NGRI, Hyderabad for permission to publish this paper. Prof. R. N. Gupta, Director and Dr G. M. Nagaraja Rao have extended co-operation and facilities for experimental tests at NIRM, Kolar Gold Field.

Received 25 April 2005; revised accepted 29 June 2005